Journal of Sound and Vibration (1998) **217**(5), 909–925
Article No. sv981802

CHARACTERIZATION OF 3D CONTACT KINEMATICS AND PREDICTION OF RESONANT RESPONSE OF STRUCTURES HAVING 3D FRICTIONAL CONSTRAINT

B. D. YANG AND C. H. MENQ

Coordinate Metrology and Measurement Laboratory,
Department of Mechanical Engineering, *The Ohio State University*,
Columbus, *OH* 43210, *U.S.A.*

(*Received* 22 *December* 1997, *and in final form* 17 *June* 1998)

A 3D friction contact model has been developed for the prediction of the resonant response of structures having 3D frictional constraint. In the proposed model, a contact plane is defined and its orientation is assumed invariant. Consequently, the relative motion of the two contacting surfaces can be resolved into two components: the in-plane tangential motion on the contact plane and the normal component perpendicular to the plane. The in-plane tangential relative motion is often two-dimensional, and it can induce stick–slip friction. On the other hand, the normal relative motion can cause variation of the contact normal load and, in extreme circumstances, separation of the two contacting surfaces. In this study, the joined effect of the 2D tangential relative motion and the normal relative motion on the contact kinematics of a friction contact is examined and analytical criteria are developed to determine the transitions among stick, slip, and separation, when experiencing variable normal load. With these transition criteria, the induced friction force on the contact plane and the variable normal load perpendicular to the plane can be predicted for any given cyclic relative motions at the contact interface and hysteresis loops can be produced so as to characterize the equivalent damping and stiffness of the friction contact. These non-linear damping and stiffness along with the harmonic balance method are then used to predict the resonant response of a frictionally constrained 3-DOF oscillator. The predicted results are compared with those of the time integration method and the damping effect, the resonant frequency shift, and the jump phenomenon are examined.

1. INTRODUCTION

Mechanical systems in which moving components are mutually constrained through frictional contacts often lead to complex contact kinematics. When examining the contact kinematics of many systems, such as turbine blade systems [1–7] and automotive clutches [8], a contact plane can usually be defined and its orientation can be assumed to be invariant when the amplitude of vibration is relatively small. Consequently, the relative motion of the two contacting surfaces can be resolved into two components: the in-plane tangential motion on the

0022–460X/98/450909 + 17 $30.00/0

contact plane and the normal component perpendicular to the contact plane. The in-plane tangential relative motion is often two-dimensional, and it can induce stick–slip friction [9, 10]. The resulting stick–slip friction often provides additional spring resistance and friction damping [11] to the system. On the other hand, the normal relative motion can cause variation of the contact normal load and, in extreme circumstances, separation of the two contacting surfaces [4, 12–14].

In the authors' earlier study [15], a simplified version of 3D contact kinematics was investigated, in which the relative motion retains the normal component that causes normal load variation, while the in-plane tangential component of the relative motion degenerates into linear motion. Based on these simplified 3D contact kinematics, a variable normal load friction force model was developed to characterize the non-linear stiffness and damping of the friction contact experiencing normal load variation and moving back and forth tangentially.

In this study, the joined effect of the 2D tangential relative motion and the normal relative motion on the contact kinematics of a friction contact is examined. This study focuses on the development of a 3D contact model which can be used to determine the effective stiffness and damping of a friction contact. Moreover, the non-linear effect of the general 3D contact kinematics on the resonant response of a frictionally constrained structure is studied. It will be shown that the stick–slip phenomenon caused by 3D contact kinematics becomes complicated due to the normal load variation, the possible interface separation, and the 2D tangential relative motion. For example, when a friction contact experiences simple contact kinematics involving linear (tangential) relative motion and contact normal load, the slip-to-stick transition can be accurately predicted using the condition when the (tangential) relative motion reverses its direction. However, when a friction contact experiences 3D contact kinematics, the ''reversion rule'' is not well defined because the contact point moves in a closed path and may never actually reverse its direction. Moreover, the normal variation also affects the occurrence of the transitions among stick, slip, and separation. Hence, the major issue in characterizing the 3D contact kinematics is to derive the necessary analytical criteria that accurately predict the transition conditions so as to assess the induced friction force.

When predicting the resonant response of a frictionally constrained structure, the induced periodic friction force along with the variable contact normal load at the friction contact can often be approximated by effective stiffness and equivalent damping over a cycle of motion. The resulting stiffness and damping can then be incorporated with the harmonic balance method to predict the forced response of a frictionally constrained structure. In this paper, a 3-DOF oscillator constrained by a friction contact is used as an example and its forced response will be calculated using the approach developed in this study. Based on the predicted results, the influences of the induced friction force and the variable contact normal load on the resonant response of a frictionally constrained structure will be discussed. The predicted results are compared with those of the time integration method and the resulting damping effect, the resonant frequency shift, and the jump phenomenon are examined.

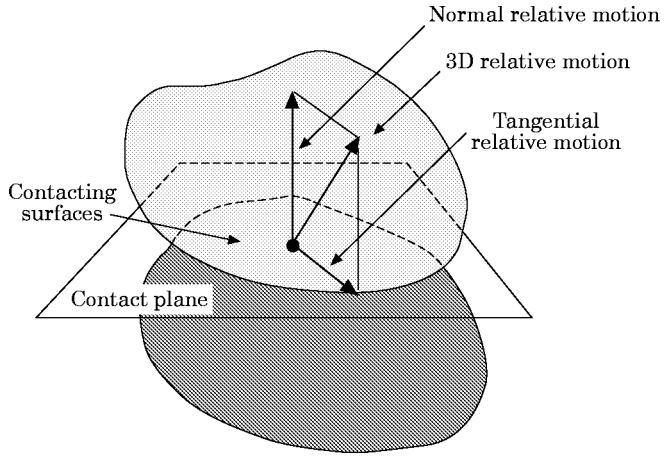

Figure 1. 3D contact kinematics.

2. 3D CONTACT KINEMATICS

Figure 1 shows two vibrating bodies mutually constrained through a frictional contact. The contact interface between these two vibrating bodies can be modelled as a substructure that contains a massless elastic element and a friction contact point, as depicted in Figure 2. The elastic element accounts for the shear and normal stiffness properties of the interface, and it is characterized by a 2×2 stiffness† matrix $\mathbf{K_u}$ for the shear stiffness† and a spring constant k_v for the normal stiffness. The friction contact point, that is assumed to obey the Coulomb friction law with the friction coefficient μ when in contact with body 2, can undergo tangential stick–slip motion, and may experience intermittent separation from

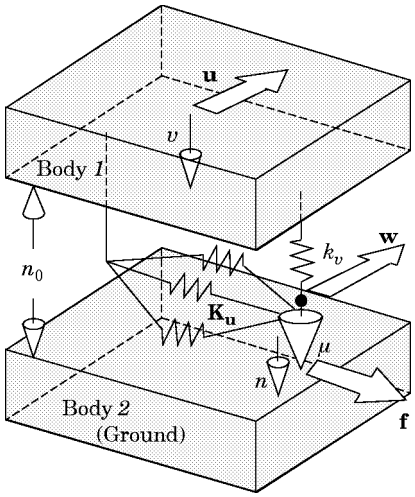

Figure 2. A model of the friction interface experiencing 3D contact kinematics.

†The 2×2 shear stiffness matrix is used because the tangential relative motion is two-dimensional. If the shear stiffness property is isotropic, a spring constant k_v can be used, and the 2×2 shear stiffness matrix becomes $k_v\mathrm{I}$, where I is the 2×2 identity matrix.

body 2 when the normal relative motion (v) becomes large. The contact interface is assumed to have either a preload or an initial gap (as designed by n_0). This model allows a negative preload to represent the situation when the interface has an initial gap; the equivalent preload across the interface with a gap e is calculated as $-k_v e$. In this model, $\mathbf{u}$ and v are the input tangential relative motion and normal relative motion of the contact interface respectively, and they can be evaluated as the motion of body 1 with respect to body 2.

2.1. CONSTRAINED FORCE

The constrained force consists of two components: the induced friction force on the contact plane and the variable normal force. Since the friction force is completely characterized by the relative motion, it will not lose generality to assume one of the contacting surfaces is the ground. With this assumption, the input tangential relative motion $\mathbf{u}$, the slip motion of the contact point $\mathbf{w}$, and the induced friction force $\mathbf{f}$ are vectors parallel to the ground; the normal relative motion v and the normal load n are scalars. The friction force, acting on the ground, can be expressed as

$$\mathbf{f} = \mathbf{K}_u(\mathbf{u} - \mathbf{w}). \tag{1}$$

The normal load is taken as the sum of the preload n_0 plus the variation caused by v, and it can be expressed as

$$n = \begin{cases} n_0 + k_v v, & \text{when } v \geqslant -n_0/k_v \\ 0, & \text{when } v < -n_0/k_v \end{cases}. \tag{2}$$

The proposed friction contact model can be applied to the most general 3D friction contact problem, where the orientation of the contact plane may oscillate when the structure vibrates. However, in this paper, its application is limited to the case, in which the orientation of the contact plane can be assumed to be invariant. In many mechanical systems, this assumption is reasonable if the amplitude of vibration is relatively small when compared to the overall dimension of the structure.

2.2. STICK, SLIP AND SEPARATION

Depending on the amplitude and phase of the various components of the vibratory motion, the friction contact will either stick, slip or separate during a cycle of oscillation. When the vibratory motion is really small, the contact point sticks and the friction force is proportional to the displacement $\mathbf{u}$ with reference to $\mathbf{w} = \mathbf{0}$, as implied in equation (2). According to the Coulomb friction law, the magnitude of the friction force is always limited by the varying slip load μn. During the course of the vibration, the interface may reach a point where the friction force tends to exceed the slip load and begin to slip. Subsequently, the friction force remains equal to the slip load, and slip takes place along the direction

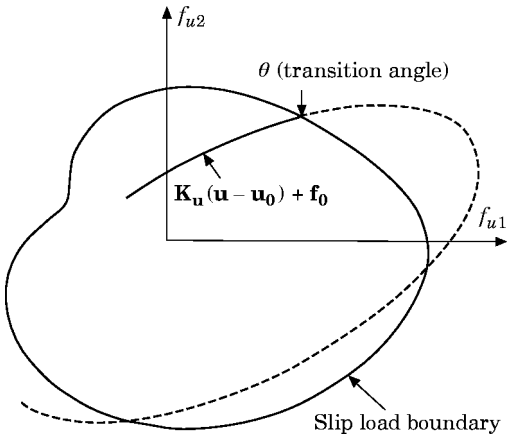

Figure 3. Stick-to-slip transition.

of the friction force until the contact point sticks again. In other words, the stick and slip conditions can be expressed as follows.

$$\text{Stick condition:} \quad |\mathbf{f} = \mathbf{K_u}(\mathbf{u} - \mathbf{u_0}) + \mathbf{f_0}| < \mu n, \quad \dot{\mathbf{w}} = \mathbf{0}; \tag{3}$$

$$\text{Slip condition:} \quad \mathbf{f} = \mu n \, \dot{\mathbf{w}}/|\dot{\mathbf{w}}|, \quad \dot{\mathbf{w}} \neq \mathbf{0}; \tag{4}$$

where $\mathbf{u}_0$ and $\mathbf{f}_0$ are the initial values of $\mathbf{u}$ and $\mathbf{f}$ at the beginning of the stick state. During the cycle of motion, the applied variable normal load may vanish to cause the interface to separate; consequently, the friction force is not present.

3. STICK/SLIP/SEPARATION TRANSITION

As mentioned, the major issue in characterizing the 3D contact kinematics is to derive the necessary analytical criteria that accurately predict the transition conditions so as to assess the induced friction force.

3.1. STICK-TO-SLIP TRANSITION

The transition occurs when $|\mathbf{f} = \mathbf{K_u}(\mathbf{u} - \mathbf{u}_0) + \mathbf{f}_0| = \mu n$. Figure 3 exemplifies graphically how the stick-to-slip transition can be obtained. In this figure, the slip load (μn) is displayed as the length of a force vector in the radial direction defined by θ. Since the normal load varies with θ, the slip load boundary is no longer a circle as in the case of constant normal load but has a varying magnitude. The transition angle θ_P^E can be found to be the moment when the trajectory $\mathbf{K_u}(\mathbf{u} - \mathbf{u}_0) + \mathbf{f}_0$ intersects with the slip load boundary. When considering an elliptical tangential relative motion $\mathbf{u} = [A \sin\theta \quad B \sin(\theta + \phi)]^{\mathrm{T}}$ and a variable normal load $n = n_0 + k_v D \sin(\theta + \psi)$, where $\theta = \omega t$, the criterion can be transformed into a quartic equation [16], whose solutions are available in analytical form [17]. Since multiple solutions may appear, the redundant solutions can be eliminated by using the constraint $|\dot{\mathbf{f}}| < \mu \dot{n}$ that guarantees the magnitude of the friction force to have a tendency to exceed the slip load.

3.2. SLIP-TO-STICK TRANSITION

The transition occurs when $\dot{\mathbf{w}} = \mathbf{0}$. However, to implement this criterion, it need be expressed in terms of the input tangential relative motion $\mathbf{u}$ and the variable normal load n. During the slip state, according to the Coulomb friction law as described in equation (4), the slip velocity of the contact plane $\dot{\mathbf{w}}$ is along the direction of the friction force,

$$\dot{\mathbf{w}} = c\mathbf{f}, \quad \text{where} \quad c > 0. \tag{5}$$

Since the magnitude of the friction force is equal to the slip load, one has

$$\mathbf{f}^{\mathrm{T}}\mathbf{f} = \mu^2 n^2. \tag{6}$$

Differentiating the above equation with respect to time gives

$$\mathbf{f}^{\mathrm{T}}\dot{\mathbf{f}} = \mu^2 n\dot{n}. \tag{7}$$

Considering equation (5) and the time differentiation of equation (1) $\dot{\mathbf{f}} = \mathbf{K}_u(\dot{\mathbf{u}} - \dot{\mathbf{w}})$, the above equation becomes

$$\mathbf{f}^{\mathrm{T}}\mathbf{K}_u\dot{\mathbf{u}} - c\mathbf{f}^{\mathrm{T}}\mathbf{K}_u\mathbf{f} = \mu^2 n\dot{n}, \tag{8}$$

or

$$c = (\mathbf{f}^{\mathrm{T}}\mathbf{K}_u\dot{\mathbf{u}} - \mu^2 n\dot{n})/\mathbf{f}^{\mathrm{T}}\mathbf{K}_u\mathbf{f}. \tag{9}$$

Therefore, from equation (5), one can obtain

$$\dot{\mathbf{w}} = [(\mathbf{f}^{\mathrm{T}}\mathbf{K}_u\dot{\mathbf{u}} - \mu^2 n\dot{n})/\mathbf{f}^{\mathrm{T}}\mathbf{K}_u\mathbf{f}]\mathbf{f}. \tag{10}$$

Substituting this equation into $\dot{\mathbf{f}} = \mathbf{K}_u(\dot{\mathbf{u}} - \dot{\mathbf{w}})$ yields

$$\dot{\mathbf{f}} = \mathbf{K}_u(\dot{\mathbf{u}} - (\mathbf{f}^{\mathrm{T}}\mathbf{K}_u\dot{\mathbf{u}}/\mathbf{f}^{\mathrm{T}}\mathbf{K}_u\mathbf{f})\mathbf{f}). \tag{11}$$

Also, from equation (10), the slip-to-stick transition criterion $\dot{\mathbf{w}} = \mathbf{0}$ implies

$$\mathbf{f}^{\mathrm{T}}\mathbf{K}_u\dot{\mathbf{u}} - \mu^2 n\dot{n} = 0. \tag{12}$$

However, it should be noted that $\mathbf{f}$ still remains undetermined at this stage. To obtain $\mathbf{f}$, the initial value problem involving equation (11) and the known initial friction force at beginning of the slip state can be solved using a numerical integration scheme such as the Runge–Kutta method. Once the friction force is obtained, the criterion (12) can be used to predict the occurrence of the slip-to-stick transition.

3.3. TRANSITION BETWEEN SEPARATION AND STICK/SLIP

The transition from stick/slip to separation occurs when the normal load vanishes. In addition, the normal load should be decreasing at this moment to guarantee the occurrence of the separation. In other words, the criterion can be expressed as

$$n = 0, \quad \dot{n} < 0. \tag{13}$$

Similarly, the separation ends when the normal load is about to develop, and therefore the moment of this occurring transition can be determined by the criterion

$$n = 0, \quad \dot{n} \geqslant 0. \tag{14}$$

After the separation ends, the interface resumes contact and its following state, either stick or slip, has to be further determined.

When the normal load and the friction force begin to develop at the end of the separation, their rates of change at this moment determine the following state. If the interface becomes stuck after the separation, according to the Coulomb friction law, the following condition has to be satisfied:

$$|\dot{\mathbf{f}} = \mathbf{K}_u \dot{\mathbf{u}}| < \mu \dot{n}. \tag{15}$$

Squaring both sides yields

$$\dot{\mathbf{u}}^T \mathbf{K}_u^T \mathbf{K}_u \dot{\mathbf{u}} < \mu^2 \dot{n}^2. \tag{16}$$

If the criterion (16) is not satisfied, that is

$$\dot{\mathbf{u}}^T \mathbf{K}_u^T \mathbf{K}_u \dot{\mathbf{u}} \geqslant \mu^2 \dot{n}^2, \tag{17}$$

the interface begins to slip after the separated surface resumes contact. It is noted that this incipient slip condition can be regarded as a one-dimensional case, because the friction force is not present at this particular moment and the slip action will be developed along $\dot{\mathbf{u}}$. Thus, according to the Coulomb friction law, the rate of change of the developing friction force can be expressed as

$$\dot{\mathbf{f}} = \mu \dot{n} \dot{\mathbf{u}} / |\dot{\mathbf{u}}|. \tag{18}$$

Once the friction force develops, it can be further determined by solving the initial value problem as described previously.

4. EFFECTIVE STIFFNESS AND DAMPING

With these transition criteria, the induced friction force on the contact plane and the variable normal load perpendicular to the contact plane can be predicted for any given cyclic relative motions at the contact point and hysteresis loops can be produced so as to characterize the equivalent damping and stiffness of the friction contact. The non-linear damping and stiffness along with the harmonic balance method can be integrated together to obtain a set of non-linear algebraic equations, which can be solved iteratively for the resonant response of a frictionally constrained structure [3, 6].

4.1. STATE-BY-STATE SIMULATION

Since the harmonic balance method will be used, the input motions are now assumed to be harmonic functions. For given elliptical tangential relative motion and harmonic normal motion, the induced steady state friction force can be attained using a "state-by-state simulation" by calculating the stick/slip/separation transitions sequentially. Figure 4 shows a typical example of the resulting friction

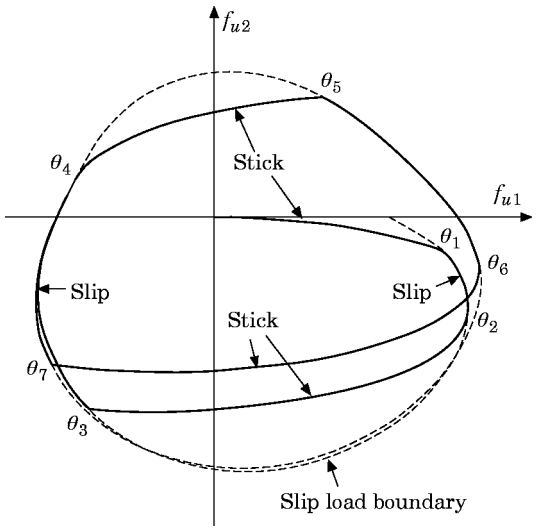

Figure 4. A friction force trajectory for the no-separation case.

force for the no-separation case. In this figure, the variable slip load, μn, is shown as a dashed trajectory. The force trajectory has several segments. Those falling on the slip load boundary correspond to slip state and the others to stick state. The simulation starts from the stick state with zero friction force; then the stick-to-slip transition angle θ_1 can be predicted by solving the corresponding stick-to-slip transition criterion, and the simulation proceeds to the slip state until the next slip-to-stick transition angle θ_2 is encountered. The simulation continues in the same manner to find the transition angles (θ_3, θ_4, . . . , etc.) until the steady state (periodic) friction force is reached. In steady state, the variable slip load also forms a closed trajectory that limits the range of the induced friction force. As can be seen from this example, the steady state friction force is attained within a few cycles. This is due to the fact that the transition angles can be accurately calculated using the analytical transition criteria developed.

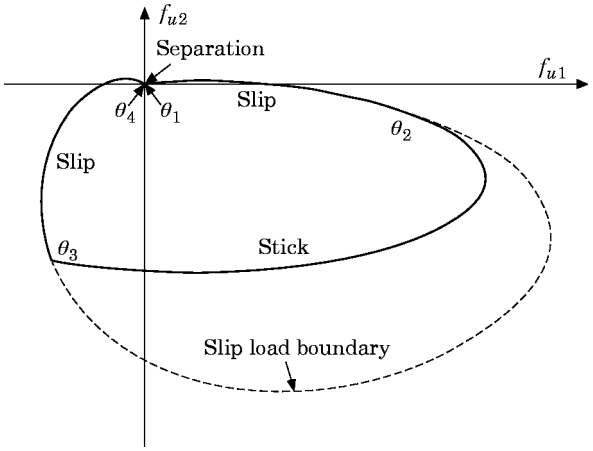

Figure 5. A friction force trajectory for the separation case.

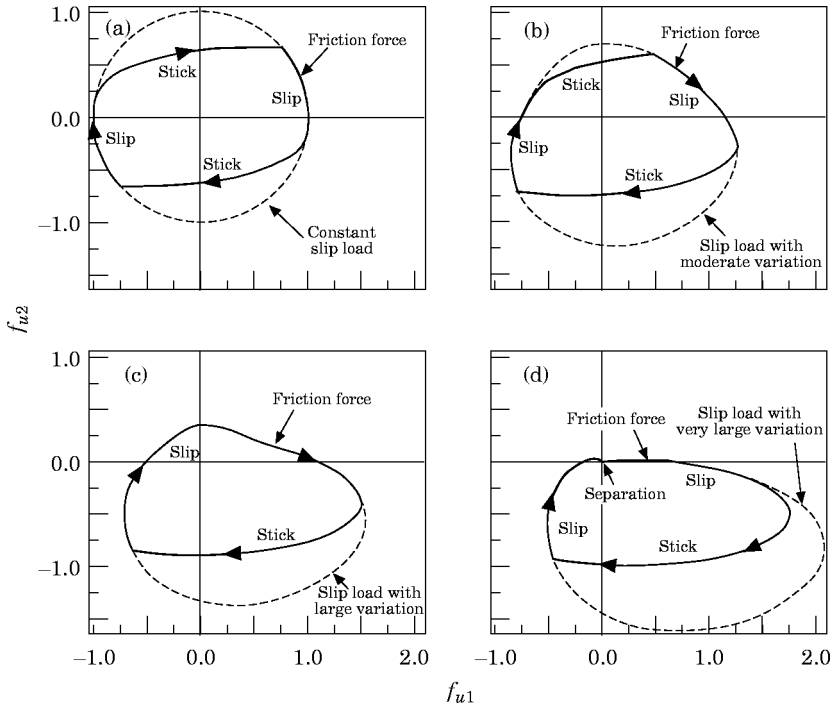

Figure 6. Friction force trajectory and applied normal load: (a) normal load is constant; (b) normal load has moderate variation; (c) normal load has large variation; (d) normal load has very large variation that causes separation.

Figure 5 shows the state-by-state simulation of a friction force trajectory having separation. Since the interval of the separation during one cycle of motion can be calculated in advance, say θ_1 for the end of the separation and θ_4 for the beginning of the separation, the steady state friction force can be reached within one cycle by performing the simulation starting from θ_1 to θ_4. As shown in this figure, the interface becomes slipping after the separation and proceeds to the stick state at θ_2. Then the stuck interface returns to the slip state again at θ_3 and keeps slipping until it separates at θ_4.

4.2. EFFECT OF NORMAL LOAD VARIATION

To demonstrate the effect of the normal load variation on the induced steady state friction force, four cases having different normal load variations are investigated, and their resulting steady state friction force trajectories are shown in Figure 6. In the case of constant normal load, the slip load (μn) is shown as a circle and the interface undergoes an alternating stick-slip motion. It can be seen that the resulting friction force trajectory is symmetrical to the origin. As the normal load variation increases to be moderate as case (b), the interface still undergoes an alternating stick-slip motion, but the resulting friction force trajectory is twisted towards the area of the greater slip load. The distortion becomes even more severe in the case of larger normal load variation. When the normal load variation is sufficiently large to cause the interface to separate for a portion of a cycle of motion as in case (d), the friction force trajectory stays at

the origin during the interval of separation as the friction force is not present, and only a part of the cyclic motion can induce the friction force. From these results, it is clear that the normal load variation can affect the induced friction force significantly and, thus, the stiffness and damping characteristics of the interface.

4.3. ESTIMATION OF STIFFNESS AND DAMPING

Once the steady state friction force is obtained, its Fourier coefficients can be calculated to estimate the time invariant term, stiffness, and damping. For input elliptical tangential relative motion and sinusoidally varying normal load, say $\mathbf{u} = [a \sin \omega t \quad b \sin(\omega t + \phi)]^{\mathrm{T}}$ and $n = n_0 + k_v c \sin(\omega t + \psi)$, the state-by-state simulation approach is used to evaluate the induced periodic friction force. Considering the time invariant term and the first harmonic terms of the Fourier series, the periodic friction force can be approximated as

$$\mathbf{f} = \begin{Bmatrix} f_{u1} \\ f_{u2} \end{Bmatrix} \approx \begin{Bmatrix} f_{b,u1} + f_{s,u1} \sin \omega t + f_{c,u1} \cos \omega t \\ f_{b,u2} + f_{s,u2} \sin(\omega t + \phi) + f_{c,u2} \cos(\omega t + \phi) \end{Bmatrix}, \tag{19}$$

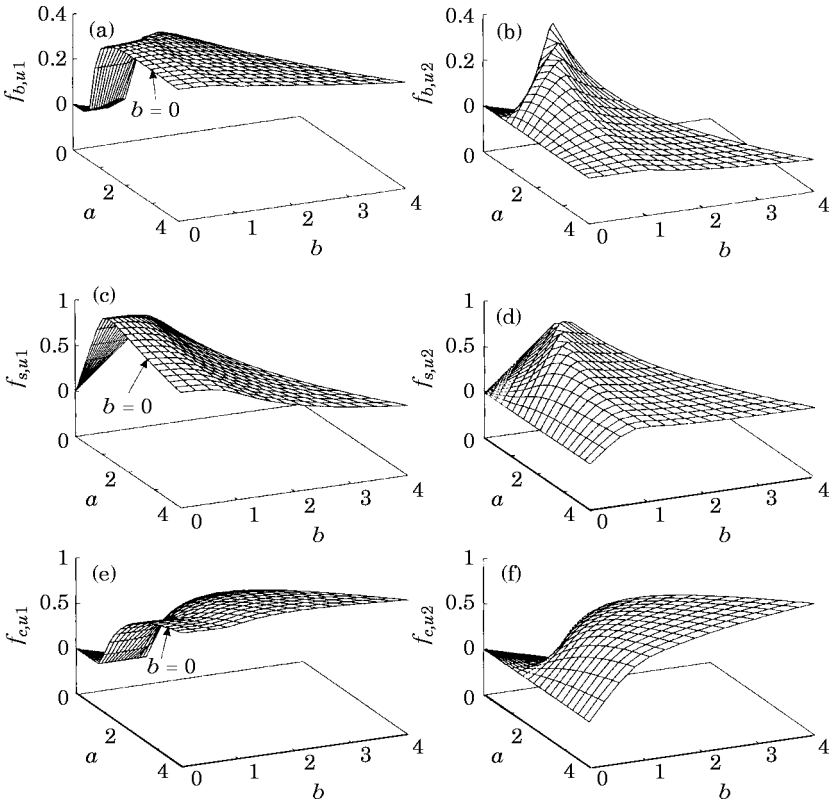

Figure 7. Predicted Fourier coefficients with a preload: (a) static component along the principal major axis; (b) static component along the principal minor axis; (c) in-phase component along the principal major axis; (d) in-phase component along the principal minor axis; (e) out-of-phase component along the principal major axis; (f) out-of-phase component along the principal minor axis.

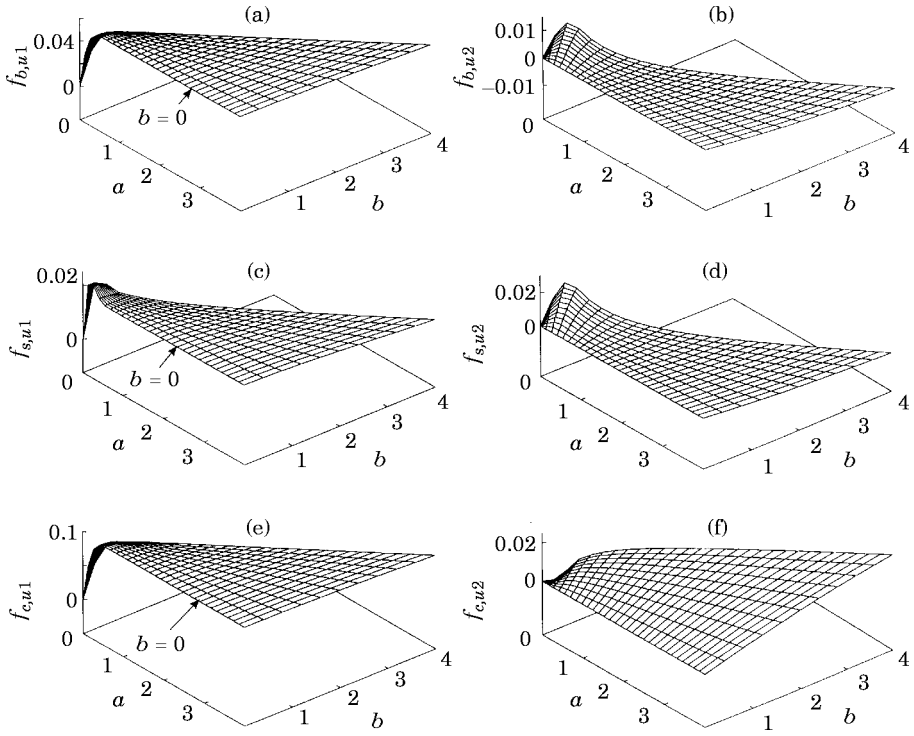

Figure 8. Predicted Fourier coefficients with an initial gap: (a) static component along the principal major axis; (b) static component along the principal minor axis; (c) in-phase component along the principal major axis; (d) in-phase component along the principal minor axis; (e) out-of-phase component along the principal major axis; (f) out-of-phase component along the principal minor axis.

where the f_s's being in phase with the motion, are the stiffness terms, and the f_c's being 90° out-of-phase, are the damping terms. Since the variable normal load results in an asymmetric friction force, the inclusion of the time invariant terms f_b becomes necessary.

Figure 7 shows calculated Fourier coefficients for a case with a preload. In this example, the directions of f_{u1} and f_{u2} are defined along the principal major and minor axes of the input elliptical tangential relative motion, respectively. Thus, the elliptical motion $\mathbf{u}$ can be expressed as $[a \sin\theta \quad b \cos\theta]^T$, in which a is the amplitude of the major axis, b the amplitude of the minor axis, and $a \geqslant b$. The predicted Fourier coefficients are plotted as functions of a and b that range within $0 \leqslant a \leqslant 4$ and $0 \leqslant b \leqslant a$. It is noticed that the boundary curves for $b = 0$ are those for the case of linear tangential relative motion that was studied in reference [15]. In this extreme case, the 2D tangential relative motion of the interface degenerates into linear motion. Similarly, Figure 8 shows calculated Fourier coefficients for a case with an initial gap.

Similarly to the friction force, the variable normal load must also be expressed as a harmonic function since it cannot contribute damping and therefore must be in phase with the input normal relative motion. The estimation of the effective stiffness of the variable normal load can be found in reference [15].

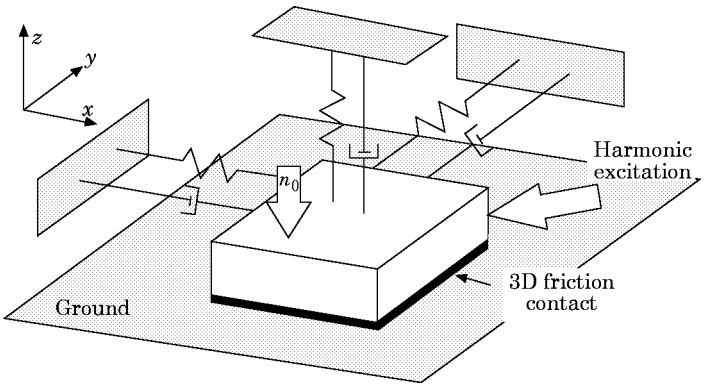

Figure 9. A 3-DOF oscillator under a friction constraint.

5. NON-LINEAR RESONANT RESPONSE

A 3-DOF oscillator is considered in this study to illustrate how the resonant response of a structure can be effected by a friction contact experiencing 3D contact kinematics. The oscillator, as depicted in Figure 9, can move in the xyz space, and either is brought into contact with the ground by a preload n_0 or has an initial gap in between. The interface between the oscillator and the ground is modelled as a flexible Coulomb friction contact, which is shown in Figure 2. When subjected to external excitation, the xy motion of the oscillator is restricted by friction, while the z motion may cause the normal load across the interface to vary. Instead of using the conventional mass–spring–dashpot notation, this 3-DOF system can be described alternatively by its modal information involving three vibration modes. It can be shown that it requires at least two vibration modes involved in the frequency range of interest to result in a response having elliptical motion in the 3D space. Therefore, to simplify the analysis, only two modes are considered, and the third mode is neglected from the analysis by assuming its natural frequency to be out of the frequency range of interest. The system parameters of the 3-DOF oscillator under investigation along with the harmonic modal excitation are shown in Table 1, in which the modal damping ratio of 0·02 represents viscous damping in the system. The parameters of the friction interface used in this investigation are: $\mu = 0{\cdot}5$, $\mathbf{K}_u = \text{diagonal } [20 \quad 20]$ and $k_v = 20$.

5.1. FORCED RESPONSE

Using the single term harmonic balance scheme along with the estimated contact force given in equation (19), a set of non-linear algebraic equations can be

TABLE 1

Modal information of the 3DOF oscillator and the excitation

Mode	Mass	Frequency (Hz)	Damping ratio	Mode shape	Excitation
1	1·0	0·9	0·02	$(1 \; 1 \; 0{\cdot}8)^T$	$1{\cdot}0 \angle 0^\circ$
2	1·0	1·1	0·02	$(1 \; -1 \; 0{\cdot}6)^T$	$1{\cdot}0 \angle 0^\circ$

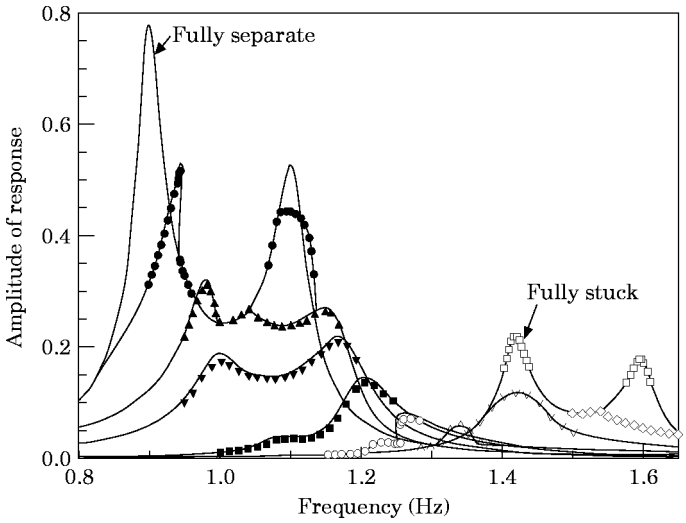

Figure 10. Forced response of the 3-DOF oscillator. n_0 values: ●, − 4; ▲, − 1; ▼, 0; ■, 1; ○, 2; ∧, 3; ∨, 5; ◇, 10; □, 32 (fully stuck).

obtained for the prediction of forced response. Under various levels of preload, the forced responses of the 3-DOF oscillator are calculated and shown in Figure 10 as continuous curves. Since the resulting responses along the three axes are similar, only the amplitude of the response along the x axis is presented in the figure. It can be observed that there exist two linear cases, which are referred to as the fully separate case and fully stuck case. The fully separate case occurs when the interface has such a large initial gap that the vibrating oscillator cannot make contact with the ground. Since the contact force is not present, two resonant responses corresponding to the natural frequencies of the system can be clearly seen. In the opposite way, when the preload of the interface exceeds some value, the interface remains fully stuck. In this case, the friction contact does not dissipate energy but provides additional stiffness, which arises from the compliance of the interface, to the system to cause higher resonant frequencies.

In between the two linear cases, the non-linear contact force, including the friction force and the variable normal load, appears to affect the response of the system. The attenuation effect of the induced friction can be clearly seen from the results. As the preload increases, the resonant response decreases until the minimum response is reached at $n_0 = 3$. Beyond this preload, the damping effect tends to reduce gradually towards the fully stuck case. The preload that minimizes response is known as the optimal preload.

As for the variable normal load, in addition to its influence on the friction characteristic, it can directly impose stiffness on the system. This non-linear stiffness arises from the intermittent separation of the contact surface during the course of vibration. It has been well known that this non-linearity can result in a multi-valued response that can lead to so called "jump phenomena" [18]. In Figure 10, two different types of jump phenomena can be clearly seen although the effect of the variable normal load is mixed with that of friction. The first one occurs when the interface has a moderate initial gap ($n_0 = -4$); as the amplitude

of the vibratory motion increases, the interface will stay in contact for some period to impose a "hardening spring" effect on the response causing the resonant peak to bend towards higher frequencies. The other jump phenomenon, however, occurs as a moderate preload is applied ($n_0 = 2$). The increase in the amplitude of the motion causes the preloaded interface to separate, and as a result, the interface cannot provide stiffness to the system temporarily. The overall effect of the temporary separation is similar to the effect of a "softening spring" that gives rise to a response with a resonance peak bending towards lower frequencies.

5.2. COMPARISON WITH TIME INTEGRATION METHOD

The comparison of the predicted results with those of the time integration method is also shown in Figure 10, in which the discrete data points denote the time integration solutions. All the comparisons are made in the frequency range near resonance. The time integration is carried out based on modal equations and the time step is determined according to the excitation frequency. In this example, there are at least 200 steps for a cycle of motion. A typical Runge–Kutta type approach is used for the numerical solution. However, when stick–slip-separation transition occurs in between two time instances, a Newton–Raphson type approach is used to search for the exact transition time. From the results, it is apparent that the approximate procedure can provide accurate solutions. This is mainly due to the fact that the superharmonic components of the periodic contact force are attenuated by the low-pass filtering effect of the structure used in this example. Therefore, the assumption of sinusoidal displacement is sufficiently accurate. When dealing with complex systems, the use of the Multi-Harmonic Balance Method [19] may be necessary. Nevertheless, a slight discrepancy can still be observed in the cases that have either small preload or small gap ($n_0 = -1, 0, 1, 2$). This is caused by the almost equal participation of the two distinct non-linearities, stick-slip friction and intermittent separation, that renders the displacement slightly off-harmonic.

5.3. JUMP PHENOMENON

As mentioned, when the gap is developed during the cycle of motion, the system may exhibit multi-valued response that causes a jump phenomenon. A typical example, occurring at $n_0 = -4$ for the system under study, is shown in Figure 11. Both solutions from the harmonic balance method and time integration method are presented. It should be noted that one of the multiple solutions from the harmonic balance method, shown as the dashed curve, is unstable [18]; separated by the unstable response, the stable response consists of two curves, which are referred to as the upper and lower branches. For the time integration method, a finer frequency increment is used in the area of interest. The multiple solutions from the time integration method can be obtained by using different initial conditions; however, the unstable solutions cannot be reached because they are not physically existent. From the time integration solutions, the multi-valued response exists between 0·9440 Hz and 0·9472 Hz.

The "jumping" behavior can be clearly seen using the time integration simulation with frequency sweeping across the jump. The simulation starts from

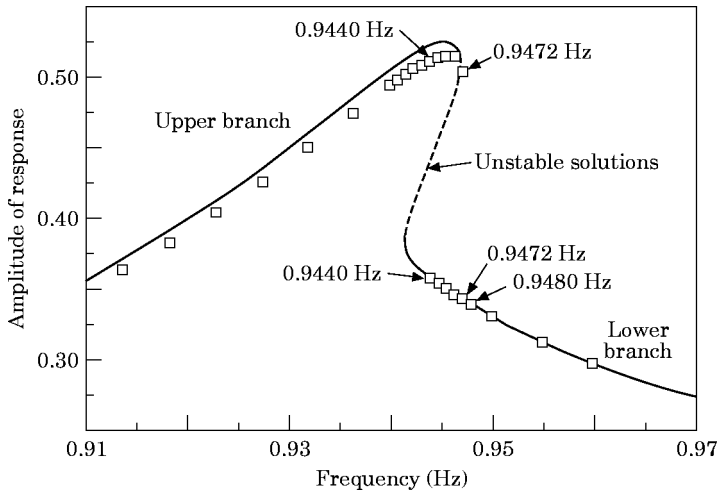

Figure 11. Response of the oscillator at $n_0 = -4$. Solid line: harmonic balance method; discrete points: time integration method.

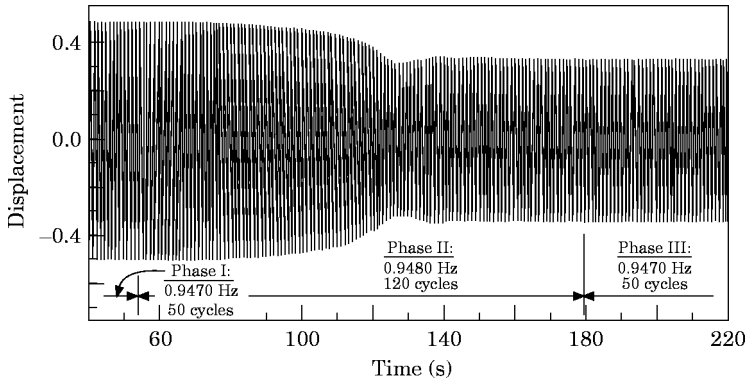

Figure 12. Time simulation of jump phenomenon.

the frequency 0·9470 Hz for 50 cycles (phase I), is then perturbed to 0·9480 Hz for 120 cycles (phase II), and finally is perturbed back to 0·9470 Hz for 50 cycles (phase III). The result is shown in Figure 12. With the selected initial condition, the displacement at the end of phase I reaches the steady state amplitude at the upper branch. In phase II, the steady state amplitude is reached after a transient period and jumps from the upper branch to the lower branch. In phase III, while the frequency is perturbed back to that of phase I, the steady state amplitude still stays in the lower branch.

6. CONCLUSIONS

A 3D friction contact model is presented in this paper. In the proposed model, the relative motion across the friction contact is resolved into two components: in-plane tangential motion on the contact plane and the normal motion component perpendicular to the plane. The in-plane tangential relative motion is

two-dimensional, and it can induce stick–slip friction. On the other hand, the normal relative motion can cause variation of the contact normal load and, in extreme circumstances, separation of the two contacting surfaces. In this paper, the joined effect of the 2D tangential relative motion and the normal relative motion on the contact kinematics of a friction contact is examined and analytical criteria are developed to determine the transitions among stick, slip, and separation, when experiencing variable normal load. Using these transition criteria, the induced friction force and the variable normal load can be predicted for any given cyclic relative motions and hysteresis loops can be produced so as to characterize the equivalent friction damping and nonlinear spring resistance of the friction contact.

These non-linear friction damping and spring resistance along with the harmonic balance method are then used to predict the resonant response of a frictionally constrained 3-DOF oscillator. The predicted results are compared with those of the time integration method and the damping effect, the resonant frequency shift, and the jump phenomenon are examined. The predicted non-linear response shows three distinct features: (1) attenuated resonant response due to stick-slip motion at the friction contact, (2) higher resonant frequency due to additional non-linear spring resistance, and (3) multi-valued response leading to jump phenomena due to intermittent interface separation.

ACKNOWLEDGMENTS

This material is based on work supported by the GUIde Consortium and the U.S. Air Force under contract No. F33615-96-C-2664. Any opinions, findings, and conclusions or recommendations expressed in this material are those of the authors and do not necessarily reflect the views of the GUIde Consortium or the Air Force.

REFERENCES

1. T. M. Cameron, J. H. Griffin, R. E. Kielb and T. M. Hoosac 1990 *Transactions of the American Society of Mechanical Engineers*, *Journal of Vibration*, *Acoustics*, *Stress and Reliability in Design* **112**, 175–182. An integrated approach for friction damper design.
2. J. H. Griffin 1980 *Transactions of the American Society of Mechanical Engineers*, *Journal of Engineering for Power* **102**, 329–333. Friction damping of resonant stresses in gas turbine engine airfoils.
3. C. H. Menq and J. H. Griffin 1985 *Transactions of the American Society of Mechanical Engineers*, *Journal of Vibration*, *Acoustics*, *Stress*, *and Reliability in Design* **107**, 19–25. A comparison of transient and steady state finite element analyses of the forced response of a frictionally damped beam.
4. C. H. Menq, J. H. Griffin and J. Bielak 1986 *Transactions of the American Society of Mechanical Engineers*, *Journal of Engineering for Gas Turbines and Power* **108**, 300–305. The influence of a variable normal load on the forced vibration of a frictionally damped structure.
5. C. H. Menq, J. H. Griffin and J. Bielak 1986 *Transactions of the American Society of Mechanical Engineers*, *Journal of Vibration*, *Acoustics*, *Stress and Reliability in Design* **108**, January, 50–55. The forced response of shrouded fan stages.

6. K. Y. Sanliturk and D. J. Ewins 1996 *Journal of Sound and Vibration* **193**, 511–523. Modelling two-dimensional friction contact and its application using harmonic balance method.
7. A. V. Srinivasan and D. G. Cutts 1983 *Transactions of the American Society of Mechanical Engineers*, *Journal of Engineering for Power* **105**, 332–341. Dry friction damping mechanisms in engine blades.
8. C. Padmanabhan 1994 *Ph.D. Dissertation*, *The Ohio State University*. Analysis of periodically excited systems with clearances.
9. J. H. Griffin and C. H. Menq 1991 *Transactions of the American Society of Mechanical Engineers*, *Journal of Vibration and Acoustics* **113**, 225–229. Friction damping of circular motion and its implications to vibration control.
10. C. H. Menq, P. Chidamparam and J. H. Griffin 1991 *Journal of Sound and Vibration* **144**, 427–447. Friction damping of two-dimensional motion and its application in vibration control.
11. A. A. Ferri 1996 *Transactions of the American Society of Mechanical Engineers*, *Journal of Vibration and Acoustics* **117**(B), 196–206. Friction damping and isolation systems.
12. J. A. C. Martins, J. T. Oden and F. M. F. Simoes 1990 *International Journal of Engineering Science* **28**, 29–92. A study of static and kinetic friction.
13. J. T. Oden and J. A. C. Martins 1985 *Computer Methods in Applied Mechanics and Engineering* **52**, 527–634. Models and computation methods for dynamic friction phenomena.
14. B. D. Yang and C. H. Menq 1997 *Transactions of the American Society of Mechanical Engineers*, *Journal of Engineering for Gas Turbines and Power* **119**, 958–963. Modeling of friction contact and its application to the design of shroud contact.
15. B. D. Yang, M. L. Chu and C. H. Menq 1998 *Journal of Sound and Vibration* **210**, 461–481. Stick–slip–separation analysis and nonlinear stiffness and damping characterization of friction contacts having variable normal load.
16. B. D. Yang 1996 *Ph.D. Dissertation*, *Department of Mechanical Engineering*, *The Ohio State University*. Contact kinematics of friction interfaces and applications to the prediction of resonant response of frictionally constrained turbine blades.
17. S. Neumark 1965 *Solution of Cubic and Quartic Equations*. NY: Pergamon Press.
18. V. T. Thomson 1981 *Theory of Vibration with Applications*. Englewood Cliffs, NJ: Prentice-Hall.
19. J. Guillen and C. Pierre 1996 *Proceedings of the* 1996 *ASME IMECE*, Atlanta, GA, November 17–22. Analysis of forced response of dry-friction damped structural system using an efficient hybrid frequency-time method.